TECHNISCHE MECHANIK, Band 23, Heft 2-4, (2003), 184– 194
Manuskripteingang: 15. Oktober 2003

The Reuss Bound of the Strain Rate Potential of Viscoplastic FCC Polycrystals

T. Böhlke and A. Bertram

This paper is dedicated to the memory of Jürgen Olschewski, who passed away so early.

The Reuss bound of the strain rate potential of face-centered cubic polycrystals without texture is numerically determined for all types of stress states. The numerical results indicate a strong dependence of the potential on the determinant of the stress deviator. This dependence implies that the viscoplastic flow is not proportional to the stress deviator. A simple analytical expression is found, which reproduces the numerical findings over a wide range of strain rate sensitivities.

1 Introduction

The distribution of crystal orientations is an important microstructural feature which affects the overall properties of polycrystalline metals. If this distribution is inhomogeneous, the material is said to have a crystallographic texture. Such a texture influences the overall elastic and the viscoplastic behavior as well as the non-mechanical properties. In the present work, the viscoplastic properties of a nontextured aggregate of face-centered cubic (fcc) crystals are considered. The advantage of a viscoplastic modeling is that on both the grain scale as well as on the macro scale the constitutive equations are given by potential relations. Furthermore, the methods of statistical continuum mechanics allow to bound the macroscopic potentials. In the most simple case, the one-point correlation function of crystal orientations is taken into account, which contains only the volume fraction information of the microstructural features. The corresponding bounds are called elementary bounds. If there is a large phase contrast on the microscale, then the elementary bounds give poor estimates of the macroscopic potentials. The incorporation of two-point and higher-order correlation functions allows to tighten the bounds. The exploitation of these second- and higher-order bounds requires a considerable computational effort.

In the present paper only the one-point correlation function of crystal orientations is taken into account. This function is called crystallite orientation distribution function in texture analysis. It specifies the volume fraction of crystals having a specific orientation. In the case of an isotropic polycrystal, this distribution function is simply constant and equal to one. Due to the high nonlinearity of the constitutive potential relations at room temperature, it is a nontrivial task to estimate the effective potentials, even in the isotropic case. The considerations here are further restricted to the isotropic Reuss bound. This bound is based on the assumption that the stress field is homogeneous over the aggregate. For the special case of a linear-viscous behavior the Reuss bound predicts a Mises type flow behavior whereas for the special case of a rate-independent behavior a Tresca type flow potential is obtained.

The main result of this paper is the numerical determination of the Reuss bound of viscoplastically isotropic polycrystals for *all* types of stress states. The bound is numerically determined by means of an adaptive integration scheme. The numerical results indicate a strong dependence of the Reuss potential on the determinant of the stress deviator. This dependence implies that the viscoplastic flow is not proportional to the stress deviator. A simple analytical expression is found, which reproduces the numerical findings over a wide range of strain rate

sensitivities. It contains the Mises type flow behavior as a special case.

Notation. Throughout the text a direct tensor notation is preferred. The scalar product, the dyadic product, and the Frobenius norm are denoted by $\boldsymbol{A} \cdot \boldsymbol{B} = \mathrm{tr}(\boldsymbol{A}^{\mathsf{T}}\boldsymbol{B})$, $\boldsymbol{A} \otimes \boldsymbol{B}$, and $\|\boldsymbol{A}\| = (\boldsymbol{A} \cdot \boldsymbol{A})^{1/2}$, respectively. Irreducible, i.e., completely symmetric and traceless tensors are designated by a prime, e.g., $\boldsymbol{A}'$ and $\mathbb{C}'$. The symmetric and the skew part of a 2nd-order tensor $\boldsymbol{A}$ are denoted by $\mathrm{sym}(\boldsymbol{A})$ and $\mathrm{skw}(\boldsymbol{A})$, respectively. Volume and orientational averages are indicated by $\langle\cdot\rangle$.

2 The Strain Rate and Stress Potentials on the Microscale

Flow Rule and Lattice Spin. Elastic distortions are assumed to be negligible. Viscoplastic deformations are considered to result from inelastic deformations in slip systems and, hence, are volume preserving. The slip rate is assumed to be driven by the resolved shear stress in the corresponding slip system. Therefore, it depends only on the deviatoric part of the stress tensor. The constitutive relation between the mass density and the hydrostatic pressure is not considered here, since only the isotropic viscoplastic behavior of an fcc polycrystal is of interest.

Distortions of viscoplastic single crystals can be modeled by the following set of equations

$$\begin{aligned} \boldsymbol{0} &= \boldsymbol{D}' - \boldsymbol{Q}\,\mathrm{sym}(\tilde{\boldsymbol{K}}(\boldsymbol{Q}^{\mathsf{T}}\boldsymbol{\tau}'\boldsymbol{Q}, \tau_\alpha^C))\boldsymbol{Q}^{\mathsf{T}}, \\ \dot{\boldsymbol{Q}}\boldsymbol{Q}^{-1} &= \boldsymbol{W} - \boldsymbol{Q}\,\mathrm{skw}(\tilde{\boldsymbol{K}}(\boldsymbol{Q}^{\mathsf{T}}\boldsymbol{\tau}'\boldsymbol{Q}, \tau_\alpha^C))\boldsymbol{Q}^{\mathsf{T}} \end{aligned} \tag{1}$$

(see, e.g., Hutchinson, 1976). $\boldsymbol{D}$ and $\boldsymbol{W}$ are the symmetric and the skew part of the velocity gradient $\boldsymbol{L} = \partial\boldsymbol{v}/\partial\boldsymbol{x}$. $\boldsymbol{\tau}$ denotes Kirchhoff stress tensor, which is related to the Cauchy stress tensor $\boldsymbol{\sigma}$ by $\boldsymbol{\tau} = J\boldsymbol{\sigma}$, where $J = \varrho_0/\varrho$ is the determinant of the deformation gradient. The internal variables τ_α^C are the critical resolved shear stresses in the different slip systems. In the present work, fcc single crystals are considered. For this specific class of materials, it is a reasonable assumption that the slip systems harden in an isotropic manner, i.e. $\tau_\alpha^C = \tau^C$ (Kocks and Mecking, 2003).

The orientation of a crystallite is described by a proper orthogonal tensor $\boldsymbol{Q} = \boldsymbol{g}_i \otimes \boldsymbol{e}_i$ where $\boldsymbol{e}_i$ and $\boldsymbol{g}_i$ represent a orthonormal basis fixed to the sample and to the (orthonormal) lattice vectors of the crystal, respectively. For a given strain rate tensor $\boldsymbol{D}'$, eqn. $(1)_1$ is an implicit equation for the stress deviator $\boldsymbol{\tau}'$. For given $\boldsymbol{\tau}'$, $\boldsymbol{W}$ and $\boldsymbol{Q}$, respectively, eqn. $(1)_2$ determines the spin $\dot{\boldsymbol{Q}}\boldsymbol{Q}^{-1}$ of the crystal lattice.

The function $\tilde{\boldsymbol{K}}$ is assumed to be given by

$$\tilde{\boldsymbol{K}}(\boldsymbol{Q}^{\mathsf{T}}\boldsymbol{\tau}'\boldsymbol{Q}, \tau^C) = \sum_\alpha^N \dot{\gamma}_\alpha(\tau_\alpha, \tau^C)\tilde{\boldsymbol{M}}_\alpha, \qquad \dot{\gamma}_\alpha(\tau_\alpha, \tau^C) = \dot{\gamma}_0 \mathrm{sign}\,(\tau_\alpha)\left|\frac{\tau_\alpha}{\tau^C}\right|^n \qquad \tau_\alpha = (\boldsymbol{Q}^{\mathsf{T}}\boldsymbol{\tau}'\boldsymbol{Q}) \cdot \tilde{\boldsymbol{M}}_\alpha \tag{2}$$

(Hutchinson, 1976). τ_α is the resolved shear stress in a slip system α. The material parameter n quantifies the strain rate sensitivity of the material. It is generally temperature dependent and can be estimated by strain rate jump experiments. At room temperature n is usually in the range $50 - 250$. In the limit $n \to \infty$ a rate-independent behavior is obtained. The Schmid or slip system tensors $\tilde{\boldsymbol{M}}_\alpha = \tilde{\boldsymbol{d}}_\alpha \otimes \tilde{\boldsymbol{n}}^\alpha$ are rank-one tensors, which are defined in terms of the slip system directions $\tilde{\boldsymbol{d}}_\alpha$ and the slip plane normals $\tilde{\boldsymbol{n}}^\alpha$. In the case of an fcc single crystal at room temperature, the octahedral slip systems $\langle 1\bar{1}0\rangle\{111\}$ have to be taken into account ($N = 12$).

Strain Rate Potential. The specification of the flow rule in eqn. (2) implies the existence of a potential Ψ^τ for $\boldsymbol{D}'$

$$\boldsymbol{D}' = \boldsymbol{H}^\tau(\boldsymbol{\tau}', \boldsymbol{Q}, \tau^C) = \frac{\partial\Psi^\tau(\boldsymbol{Q}^{\mathsf{T}}\boldsymbol{\tau}'\boldsymbol{Q}, \tau^C)}{\partial\boldsymbol{\tau}'}, \tag{3}$$

where

$$\Psi^\tau(\boldsymbol{Q}^{\mathsf{T}}\boldsymbol{\tau}'\boldsymbol{Q}, \tau^C) = \frac{1}{n+1}\sum_\alpha \dot{\gamma}_0\tau^C\left|\frac{(\boldsymbol{Q}^{\mathsf{T}}\boldsymbol{\tau}'\boldsymbol{Q}) \cdot \tilde{\boldsymbol{M}}_\alpha}{\tau^C}\right|^{n+1}. \tag{4}$$

The potential Ψ^τ is a convex function of the stress deviator $\boldsymbol{\tau}'$. Hence, there exists a one-to-one relation between $\boldsymbol{\tau}'$ and $\boldsymbol{D}'$. The functions $\boldsymbol{H}^\tau$ and Ψ^τ are homogeneous of degree n and $n+1$, respectively

$$\boldsymbol{H}^\tau(\lambda\boldsymbol{\tau}', \boldsymbol{Q}, \tau^C) = \lambda^n \boldsymbol{H}^\tau(\boldsymbol{\tau}', \boldsymbol{Q}, \tau^C) \qquad \forall\lambda > 0, \tag{5}$$

$$\Psi^\tau(\lambda\boldsymbol{Q}^\mathsf{T}\boldsymbol{\tau}'\boldsymbol{Q}, \tau^C) = \lambda^{n+1}\Psi^\tau(\boldsymbol{Q}^\mathsf{T}\boldsymbol{\tau}'\boldsymbol{Q}, \tau^C) \qquad \forall\lambda > 0. \tag{6}$$

Stress Potential. The convexity of Ψ^τ implies the existence of a potential Ψ^D for $\boldsymbol{\tau}'$ such that

$$\boldsymbol{\tau}' = \boldsymbol{H}^D(\boldsymbol{D}', \boldsymbol{Q}, \tau^C) = \frac{\partial \Psi^{\,\mathrm{D}}(\boldsymbol{Q}^\mathsf{T}\boldsymbol{D}'\boldsymbol{Q}, \tau^C)}{\partial \boldsymbol{D}'}. \tag{7}$$

Ψ^τ and Ψ^D are dual potentials and Ψ^D can be determined by a Legendre-Fenchel transformation

$$\Psi^{\,\mathrm{D}}(\boldsymbol{Q}^\mathsf{T}\boldsymbol{D}'\boldsymbol{Q}, \tau^C) = \sup_{\boldsymbol{\tau}'}(\boldsymbol{\tau}' \cdot \boldsymbol{D}' - \Psi^\tau(\boldsymbol{Q}^\mathsf{T}\boldsymbol{\tau}'\boldsymbol{Q}, \tau^C)). \tag{8}$$

The functions $\boldsymbol{H}^D$ and Ψ^D are homogeneous of degree $1/n$ and $(n+1)/n$, respectively

$$\boldsymbol{H}^D(\lambda\boldsymbol{D}', \boldsymbol{Q}, \tau^C) = \lambda^{\frac{1}{n}} \boldsymbol{H}^D(\boldsymbol{D}', \boldsymbol{Q}, \tau^C) \qquad \forall\lambda > 0, \tag{9}$$

$$\Psi^{\,\mathrm{D}}(\lambda\boldsymbol{Q}^\mathsf{T}\boldsymbol{D}'\boldsymbol{Q}, \tau^C) = \lambda^{\frac{n+1}{n}} \Psi^{\,\mathrm{D}}(\boldsymbol{Q}^\mathsf{T}\boldsymbol{D}'\boldsymbol{Q}, \tau^C) \qquad \forall\lambda > 0. \tag{10}$$

3 The Strain Rate and Stress Potentials on the Macroscale

Strain Rate Potential. In the following, a representative volume element (rve) in a statistically homogeneous fcc polycrystal is considered. An rve is a volume which is small enough to be macroscopically considered as a material point. Furthermore, an rve is large enough to contain a statistically representative volume fraction of the microstructure. The boundary of the rve and its outer normal vector are denoted by ∂v and $\boldsymbol{n}$, respectively. Both the velocity vector as well as the traction vector are assumed to be continuous on grain boundaries. Furthermore, the assumption of a homogeneous hardening state in the rve is adopted. In this section we shortly summarize the basic statements that are important in the context of the elementary bounds (see, e.g., Willis, 1989; Ponte Castañeda, 1991, 1992; Nemat-Nasser and Hori, 1999; Ponte Castañeda and Suquet, 1998; Torquato, 2002)

Let $\mathcal{B}_\tau$ be the class of trial stress fields $\check{\boldsymbol{\tau}}$ defined by the set

$$\mathcal{B}_\tau = \{\check{\boldsymbol{\tau}} : \check{\boldsymbol{\tau}}(\boldsymbol{x})\boldsymbol{n} = \bar{\boldsymbol{\tau}}\boldsymbol{n}\ \forall \boldsymbol{x} \in \partial v;\ \mathrm{div}\,(\check{\boldsymbol{\tau}}/J) = 0;\ \check{\boldsymbol{\tau}} = \check{\boldsymbol{\tau}}^\mathsf{T}\} \tag{11}$$

and let

$$\mathcal{F}_\tau(\check{\boldsymbol{\tau}}', \bar{\boldsymbol{\tau}}') = \langle \Psi^\tau(\boldsymbol{Q}^\mathsf{T}\check{\boldsymbol{\tau}}'\boldsymbol{Q}, \tau^C)\rangle \tag{12}$$

be the trial functional. Among all trial fields $\check{\boldsymbol{\tau}}'$, the field $\boldsymbol{\tau}'$ that makes the associated strain rate field compatible is the one that uniquely minimizes the trial functional $\mathcal{F}_\tau$

$$\mathcal{F}_\tau(\boldsymbol{\tau}', \bar{\boldsymbol{\tau}}') \leq \mathcal{F}_\tau(\check{\boldsymbol{\tau}}', \bar{\boldsymbol{\tau}}'), \tag{13}$$

$$\delta\mathcal{F}_\tau(\boldsymbol{\tau}', \bar{\boldsymbol{\tau}}') = 0, \qquad \delta^2\mathcal{F}_\tau(\boldsymbol{\tau}', \bar{\boldsymbol{\tau}}') = \langle \delta\boldsymbol{\tau}' \cdot \frac{\partial^2 \Psi^\tau}{\partial \boldsymbol{\tau}'^2}[\delta\boldsymbol{\tau}']\rangle \geq 0 \tag{14}$$

(Hutchinson, 1976). Furthermore, it can be shown that the average of Ψ^τ corresponding to the real field $\boldsymbol{\tau}'$

$$\bar{\Psi}^\tau(\bar{\boldsymbol{\tau}}') = \inf_{\check{\boldsymbol{\tau}}' \in \mathcal{B}_\tau} \langle \Psi^\tau(\boldsymbol{Q}^\mathsf{T}\check{\boldsymbol{\tau}}'\boldsymbol{Q}, \tau^C)\rangle \tag{15}$$

represents a potential for the average strain rate

$$\bar{\boldsymbol{D}}' = \frac{\partial \bar{\Psi}^{\tau}(\bar{\boldsymbol{\tau}}')}{\partial \bar{\boldsymbol{\tau}}'}. \tag{16}$$

Stress Potential. Let $\mathcal{B}_D$ be the class of trial strain rate fields $\check{\boldsymbol{D}}'$ with associated velocity field $\check{\boldsymbol{v}}$ defined by the set

$$\mathcal{B}_D = \{\check{\boldsymbol{D}}' : \check{\boldsymbol{v}}(\boldsymbol{x}) = \bar{\boldsymbol{D}}'\boldsymbol{x} \,\forall \boldsymbol{x} \in \partial v\,, \check{\boldsymbol{D}}' = (\operatorname{grad}(\check{\boldsymbol{v}}(\boldsymbol{x})) + \operatorname{grad}(\check{\boldsymbol{v}}(\boldsymbol{x}))^{\mathsf{T}})/2\} \tag{17}$$

and let

$$\mathcal{F}_D(\check{\boldsymbol{D}}', \bar{\boldsymbol{D}}') = \langle \Psi^D(\boldsymbol{Q}^{\mathsf{T}}\check{\boldsymbol{D}}'\boldsymbol{Q}, \tau^C)\rangle \tag{18}$$

be the trial functional. Among all trial fields $\check{\boldsymbol{D}}'$, the field $\boldsymbol{D}'$ that makes the associated stress field divergence-free and symmetric is the one that uniquely minimizes the trial functional $\mathcal{F}_D$

$$\mathcal{F}_D(\boldsymbol{D}', \bar{\boldsymbol{D}}') \leq \mathcal{F}_D(\check{\boldsymbol{D}}', \bar{\boldsymbol{D}}'), \tag{19}$$

$$\delta\mathcal{F}_D(\boldsymbol{D}', \bar{\boldsymbol{D}}') = 0, \qquad \delta^2\mathcal{F}_D(\boldsymbol{D}', \bar{\boldsymbol{D}}') = \langle \delta\boldsymbol{D}' \cdot \frac{\partial^2 \Psi^D}{\partial \boldsymbol{D}'^2}[\delta\boldsymbol{D}']\rangle \geq 0. \tag{20}$$

(Hutchinson, 1976). Furthermore, it can be shown that the average of Ψ^D corresponding to the real field $\boldsymbol{D}'$

$$\bar{\Psi}^D(\bar{\boldsymbol{D}}') = \inf_{\check{\boldsymbol{D}}' \in \mathcal{B}_D} \langle \Psi^D(\boldsymbol{Q}^{\mathsf{T}}\check{\boldsymbol{D}}'\boldsymbol{Q}, \tau^C)\rangle \tag{21}$$

represents a potential for the average stress

$$\bar{\boldsymbol{\tau}}' = \frac{\partial \bar{\Psi}^D(\bar{\boldsymbol{D}}')}{\partial \bar{\boldsymbol{D}}'}. \tag{22}$$

The potentials $\bar{\Psi}^D(\bar{\boldsymbol{D}}')$ and $\bar{\Psi}^{\tau}(\bar{\boldsymbol{\tau}}')$ are not dual to each other in general, because the corresponding boundary conditions are different (Willis, 1989; Ponte Castañeda, 1991, 1992)

$$\bar{\Psi}^D(\bar{\boldsymbol{D}}') \geq \sup_{\bar{\boldsymbol{\tau}}'} \left(\bar{\boldsymbol{\tau}}' \cdot \bar{\boldsymbol{D}}' - \bar{\Psi}^{\tau}(\bar{\boldsymbol{\tau}}')\right). \tag{23}$$

Elementary Bounds. In the context of a viscoplastic material behavior it is possible to derive upper and lower bounds for the overall strain rate potential and the overall stress potential. The most simple estimates, the so called elementary bounds, are based on the one-point statistics of the microstructure. The one-point correlation functions represent only the volume fraction information of the microstructure. The advantage of the elementary bounds is that they can be computed quite easily since no boundary-value problem has to be solved. These bounds are only accurate for small phase contrasts on the microscale. The larger the phase contrast on the microscale is, the larger is the distance between the bounds. The incorporation of higher-order correlation functions allows to tighten the bounds. For the incorporation of higher-order bounds see for example Beran (1968), Nemat-Nasser and Hori (1999), Ponte Castañeda and Suquet (1998), Torquato (2002).

The Reuss Bound. It immediately follows from eqn. (15) that the assumption of a homogeneous stress field (Sachs, 1928; Reuss, 1929) gives a bound for the strain rate potential

$$\bar{\Psi}^{\tau}(\bar{\boldsymbol{\tau}}') \leq \bar{\Psi}^R(\bar{\boldsymbol{\tau}}') = \langle \Psi^{\tau}(\boldsymbol{Q}^{\mathsf{T}}\bar{\boldsymbol{\tau}}'\boldsymbol{Q}, \tau^C)\rangle. \tag{24}$$

The dual potential is obtained by a Legendre-Fenchel transformation

$$\bar{\Psi}^{R*}(\bar{\boldsymbol{D}}') = \sup_{\bar{\boldsymbol{\tau}}'} \left(\bar{\boldsymbol{\tau}}' \cdot \bar{\boldsymbol{D}}' - \bar{\Psi}^R(\bar{\boldsymbol{\tau}}')\right). \tag{25}$$

The Reuss bound predicts the following rate of deformation

$$\bar{\boldsymbol{D}}'^{R} = \frac{\partial \bar{\Psi}^{R}(\bar{\boldsymbol{\tau}}')}{\partial \bar{\boldsymbol{\tau}}'}. \tag{26}$$

The Voigt Bound. It immediately follows from eqn. (21) that the assumption of a homogeneous strain rate field (Voigt, 1889; Taylor, 1938; Bishop and Hill, 1951; Hutchinson, 1976) gives a bound for the stress potential

$$\bar{\Psi}^{D}(\bar{\boldsymbol{D}}') \leq \bar{\Psi}^{V}(\bar{\boldsymbol{D}}') = \langle \Psi^{D}(\boldsymbol{Q}^{\mathsf{T}} \bar{\boldsymbol{D}}' \boldsymbol{Q}, \tau^{C}) \rangle. \tag{27}$$

The dual potential is obtained by a Legendre-Fenchel transformation

$$\bar{\Psi}^{V*}(\bar{\boldsymbol{\tau}}') = \sup_{\bar{\boldsymbol{D}}'} \left(\bar{\boldsymbol{\tau}}' \cdot \bar{\boldsymbol{D}}' - \bar{\Psi}^{V}(\bar{\boldsymbol{D}}') \right). \tag{28}$$

The Voigt bound predicts the following stress tensor

$$\bar{\boldsymbol{\tau}}'^{V} = \frac{\partial \bar{\Psi}^{V}(\bar{\boldsymbol{D}}')}{\partial \bar{\boldsymbol{D}}'}. \tag{29}$$

The following relations hold for sufficiently large representative volume elements

$$\bar{\Psi}^{V*}(\bar{\boldsymbol{\tau}}') \leq \bar{\Psi}^{\tau}(\bar{\boldsymbol{\tau}}') \leq \bar{\Psi}^{R}(\bar{\boldsymbol{\tau}}'), \tag{30}$$

$$\bar{\Psi}^{R*}(\bar{\boldsymbol{D}}') \leq \bar{\Psi}^{D}(\bar{\boldsymbol{D}}') \leq \bar{\Psi}^{V}(\bar{\boldsymbol{D}}'). \tag{31}$$

The Voigt estimate $\bar{\Psi}^{V*}$ represents a lower bound whereas the Reuss estimate $\bar{\Psi}^{R}$ is an upper bound for the strain rate potential $\bar{\Psi}^{\tau}$.

4 Numerical Approximation of the Isotropic Reuss Bound

Homogenization Based on Orientation Averages. The distribution of crystal orientations $\boldsymbol{Q}$ can be quantitatively described by the crystallite orientation distribution function $f(\boldsymbol{Q})$ (Bunge, 1965; Roe, 1965). The function $f(\boldsymbol{Q})$ specifies the volume fraction $\mathrm{d}v/v$ of crystals having the orientation $\boldsymbol{Q}$, i.e.

$$\frac{\mathrm{d}v}{v}(\boldsymbol{Q}) = f(\boldsymbol{Q})\,\mathrm{d}Q. \tag{32}$$

$\mathrm{d}Q$ is the volume element in $SO(3)$ which ensures an invariant integration over $SO(3)$ (Gel'fand et al., 1963), i.e.

$$\int_{SO(3)} f(\boldsymbol{Q})\,\mathrm{d}Q = \int_{SO(3)} f(\boldsymbol{Q}\boldsymbol{Q}_0)\,\mathrm{d}Q \qquad \forall \boldsymbol{Q}_0 \in SO(3). \tag{33}$$

If $SO(3)$ is parameterized by Euler angles, the volume element $\mathrm{d}Q$ is given by

$$\mathrm{d}Q = \frac{\sin(\Phi)}{8\pi^2}\,\mathrm{d}\varphi_1\,\mathrm{d}\Phi\,\mathrm{d}\varphi_2. \tag{34}$$

The function $f(\boldsymbol{Q})$ is nonnegative and normalized such that

$$f(\boldsymbol{Q}) \geq 0 \qquad \forall \boldsymbol{Q} \in SO(3), \qquad \int_{SO(3)} f(\boldsymbol{Q})\,\mathrm{d}Q = 1. \tag{35}$$

The orientation distribution function $f(\boldsymbol{Q})$ reflects both the symmetry of the crystallites forming the aggregate and the sample symmetry, which results from the processing history (Zheng and Fu, 2001). The crystal symmetry

implies the following symmetry relation for $f(\boldsymbol{Q})$

$$f(\boldsymbol{Q}) = f(\boldsymbol{Q}\boldsymbol{H}^C) \qquad \forall \boldsymbol{H}^C \in S^C \subseteq SO(3). \tag{36}$$

S^C denotes the symmetry group of the crystallite. The sample symmetry implies the following symmetry relation for $f(\boldsymbol{Q})$

$$f(\boldsymbol{Q}) = f(\boldsymbol{H}^S\boldsymbol{Q}) \qquad \forall \boldsymbol{H}^S \in S^S \subseteq SO(3). \tag{37}$$

S^S denotes the symmetry group of the sample.

Let $\psi(\boldsymbol{Q}(\boldsymbol{x}))$ be a mechanical quantity of a crystallite which depends on the position vector only by its dependence on the orientation $\boldsymbol{Q}$. Volume averages of such a quantity can be transformed by equation (32) into averages over $SO(3)$

$$\bar{\psi} = \frac{1}{v}\int_v \psi(\boldsymbol{Q}(\boldsymbol{x}))\,\mathrm{d}v = \int_{SO(3)} f(\boldsymbol{Q})\psi(\boldsymbol{Q})\,\mathrm{d}Q. \tag{38}$$

Parameterization of the Stress Deviator. The stress deviator $\bar{\boldsymbol{\tau}}'$ can generally be decomposed into

$$\bar{\boldsymbol{\tau}}' = \|\bar{\boldsymbol{\tau}}'\|\boldsymbol{Q}_\tau\boldsymbol{N}'_\tau\boldsymbol{Q}_\tau^{\mathsf{T}}, \tag{39}$$

where $\|\bar{\boldsymbol{\tau}}'\|$ is the magnitude of $\bar{\boldsymbol{\tau}}'$. $\boldsymbol{Q}_\tau$ is an orthogonal tensor that maps an arbitrary orthonormal reference bases $\boldsymbol{e}_i$ onto the eigenvectors of $\bar{\boldsymbol{\tau}}'$. The eigenvectors of the symmetric tensor $\boldsymbol{N}'_\tau$ are $\boldsymbol{e}_i$ and the eigenvalues n_α of $\boldsymbol{N}'_\tau$ are equal to those of $\bar{\boldsymbol{\tau}}'$ divided by $\|\bar{\boldsymbol{\tau}}'\|$. The restrictions $\mathrm{tr}(\boldsymbol{N}'_\tau) = 0$ and $\|\boldsymbol{N}'_\tau\| = 1$ hold. As a result, the eigenvalues n_α are constrained by $n_1 + n_2 + n_3 = 0$ and $n_1^2 + n_2^2 + n_3^2 = 1$, respectively. These constraints are identically fulfilled by the following parameterization of $\boldsymbol{N}'_\tau$

$$\boldsymbol{N}'_\tau(\xi) = \sum_{\alpha=1}^{3} n_\alpha \boldsymbol{e}_\alpha \otimes \boldsymbol{e}_\alpha, \qquad n_{1,3} = -\frac{\sqrt{6}}{6}\xi \pm \frac{\sqrt{2}}{2}\sqrt{1-\xi^2}, \qquad n_2 = \frac{\sqrt{6}}{3}\xi, \tag{40}$$

$\xi \in [-1/2, +1/2]$. The principal invariants of $\bar{\boldsymbol{\tau}}'$ are

$$I = 0, \qquad II = -\frac{1}{2}\|\bar{\boldsymbol{\tau}}'\|^2, \qquad III = \frac{\sqrt{6}}{6}\|\bar{\boldsymbol{\tau}}'\|^3\xi\left(\frac{4}{3}\xi^2 - 1\right). \tag{41}$$

The principal invariants of $\boldsymbol{N}'_\tau$ are

$$I^* = 0, \qquad II^* = -\frac{1}{2}, \qquad III^* = \frac{\sqrt{6}}{6}\xi\left(\frac{4}{3}\xi^2 - 1\right) \in [-\frac{\sqrt{6}}{18}, +\frac{\sqrt{6}}{18}]. \tag{42}$$

In the case of an isotropic body, the ξ-values $-1/2$, 0, and $+1/2$ belong to the stress states corresponding to uniaxial elongation, plane strain compression, and simple compression, respectively.

The Isotropic Reuss Bound. In this section the Reuss bound for the strain rate potential of an isotropic fcc polycrystal is numerically determined. In the case of the Reuss bound, the stress field is assumed to be homogeneous over the polycrystal, i.e. $\bar{\boldsymbol{\tau}}' = \boldsymbol{\tau}'$. According to (24) the Reuss bound is given by

$$\bar{\Psi}^R(\bar{\boldsymbol{\tau}}') = \langle \Psi^\tau(\boldsymbol{Q}^{\mathsf{T}}\bar{\boldsymbol{\tau}}'\boldsymbol{Q}, \tau^C)\rangle = \int_{SO(3)} f(\boldsymbol{Q})\Psi^\tau(\boldsymbol{Q}^{\mathsf{T}}\bar{\boldsymbol{\tau}}'\boldsymbol{Q}, \tau^C)\,\mathrm{d}Q. \tag{43}$$

The isotropy of the polycrystal is equivalent to $f(\boldsymbol{Q}) = 1$ and the last equation can be simplified to

$$\bar{\Psi}^{RI}(\bar{\boldsymbol{\tau}}') = \int_{SO(3)} \Psi^\tau(\boldsymbol{Q}^{\mathsf{T}}\bar{\boldsymbol{\tau}}'\boldsymbol{Q}, \tau^C)\,\mathrm{d}Q. \tag{44}$$

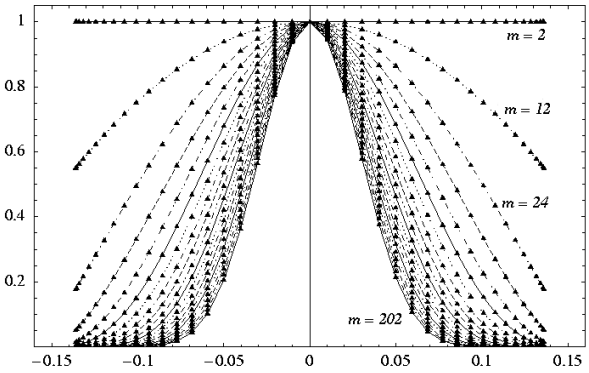

Figure 1: $\Gamma^*(III^*, m)$ determined by a numerical integration of eqn. (46) vs III^* for different values of m $(2, 12, 24, \ldots, 202)$

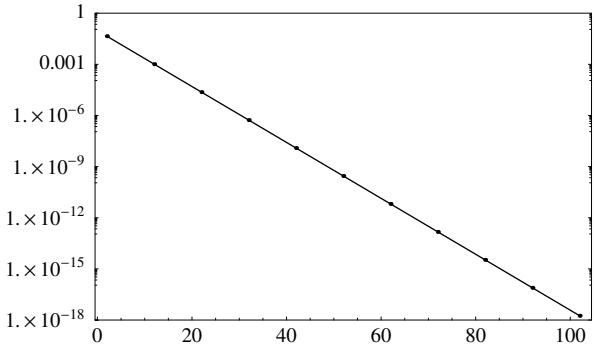

Figure 2: $\Gamma(0, m)$ determined by a numerical integration of eqn. (46) vs m (points) and $\Gamma(0, m) \approx 10^{a-b(m-2)}$ vs m with $a = -1.35$, $b = 0.164$ (solid line)

After introducing the strain rate potential of fcc single crystals (see (4)), the Reuss bound is given by

$$\bar{\Psi}^{RI}(\bar{\boldsymbol{\tau}}') = \frac{\dot{\gamma}_0 \tau^C N}{m} \left(\frac{\|\bar{\boldsymbol{\tau}}'\|}{\tau^C} \right)^m \Gamma(III^*, m), \qquad m = n + 1, \tag{45}$$

where

$$\Gamma(III^*, m) = \int_{SO(3)} \left| \boldsymbol{N}'_\tau(\xi(III^*)) \cdot \boldsymbol{Q}\tilde{\boldsymbol{M}}\boldsymbol{Q}^{\mathsf{T}} \right|^m \mathrm{d}Q. \tag{46}$$

N denotes the number of slip systems. Due to the isotropy of the aggregate only one arbitrary Schmid tensor $\tilde{\boldsymbol{M}}$ of the twelve tensors $\tilde{\boldsymbol{M}}_\alpha$ has to be considered in the integral. The homogeneity properties of the potential function Ψ^τ imply that $\bar{\Psi}^{RI}$ is homogeneous of degree m in $\|\bar{\boldsymbol{\tau}}'\|$. It is important to note that the integral in (46) only depends on the principal invariant $III^* \in [-\sqrt{6}/18, +\sqrt{6}/18]$ of $\boldsymbol{N}'_\tau$ and on the material parameter $m \in [2, \infty]$. Without loss of generality, the integral (46) can be written in form of

$$\Gamma(III^*, m) = \Gamma(0, m)\Gamma^*(III^*, m). \tag{47}$$

It can be seen that the isotropic Reuss bound is described by the two functions $\Gamma(0, m)$ and $\Gamma^*(III^*, m)$, respectively.

In Fig. 1 the numerical approximation of the function $\Gamma^*(III^*, m)$ is plotted for different values of m in the interval $[-\sqrt{6}/18, +\sqrt{6}/18]$. The numerical integration over $SO(3)$ has been performed by means of an adaptive integration scheme (Berntsen and Espelid, 1991a,b). It can be seen that only for $m = 2$ the Reuss bound is independent of III^*. For larger values of m, a strong dependence of the effective potential on the determinant of $\boldsymbol{N}'_\tau$ is observed. In Fig. 2 discrete values of $\Gamma(0, m)$ are plotted for different values of m. Note that for the numerical determination of the functions $\Gamma(0, m)$ and $\Gamma^*(III^*, m)$, a normalization must be performed in order to capture the order of magnitude of the two functions.

In Fig. 3 the function $\operatorname{arccosh}(1 - \ln(\Gamma^*(III^*, m)))$ is shown. The plot of the transformed function, which shows an almost linear dependence on III^* for all values of m, motivates the following ansatz

$$\Gamma^*(III^*, m) \approx \exp(1 - \cosh(\beta(m) \,|\, III^* \,|)), \tag{48}$$

which is used in order to find the optimal $\beta(m)$ for fixed m. This is done by means of a least-squares fit based on the Levenberg-Marquardt method. As a result one obtains a set of discrete values of β over m shown in Fig. 4. The discrete values can be approximated by the following ansatz

$$\beta(m) \approx c\sqrt{m - 2}, \qquad c = 2.294, \tag{49}$$

where the numerical value of a has also been obtained by the aforementioned optimization scheme. The numerical

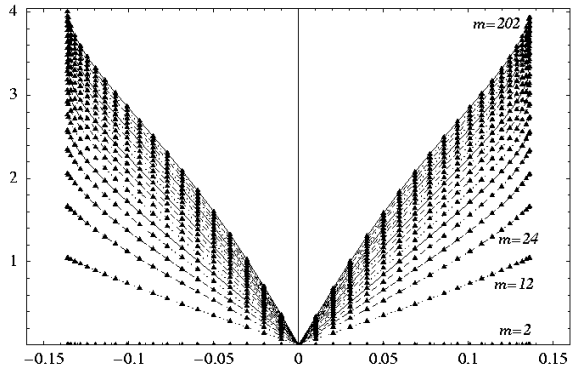

Figure 3: $\operatorname{arccosh}(1-\ln(\Gamma^*(III^*,m)))$ determined by numerical integration of eqn. (46) vs III^* for different values of m $2, 12, 24, \ldots, 202$

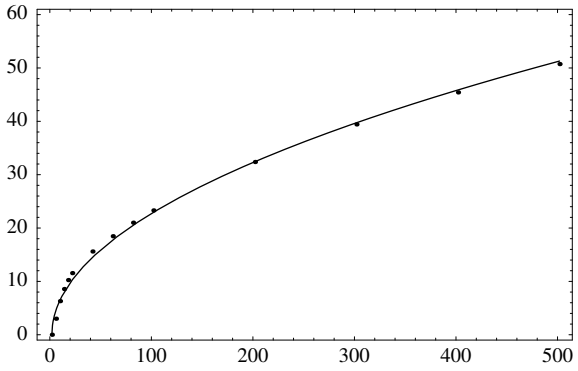

Figure 4: $\beta(m)$ determined by a least-squares fit of the numerical data (see, Fig. 1) (points) and $\beta(m) \approx 2.294\sqrt{m-2}$ (solid line)

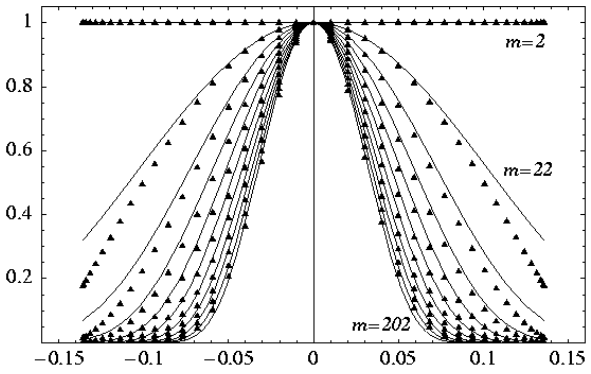

Figure 5: $\Gamma^*(III^*,m)$ vs III^* for different values of m $(2, 22, 42, \ldots, 202)$: determined by numerical integration of eqn. (46) (triangles) and approximated by $\Gamma^*(III^*,m) \approx \exp(1-\cosh(\beta(m)\,|\,III^*\,|))$ (solid lines)

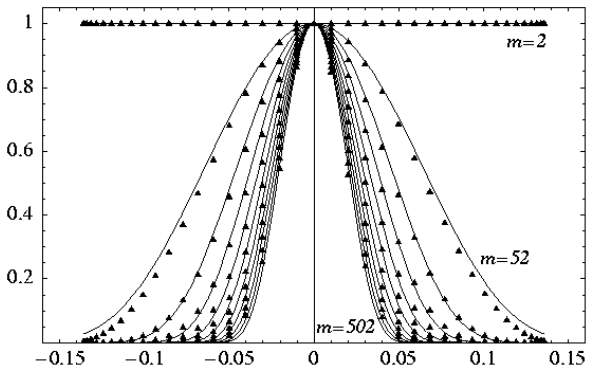

Figure 6: $\Gamma^*(III^*,m)$ vs III^* for different values of m $(2, 52, 102, \ldots, 502)$: determined by numerical integration of eqn. (46) (triangles) and approximated by $\Gamma^*(III^*,m) \approx \exp(1-\cosh(\beta(m)\,|\,III^*\,|))$ (solid lines)

constants in the following ansatz for $\Gamma(0,m)$

$$\Gamma(0,m) \approx 10^{a-b(m-2)}, \qquad a=-1.35, \qquad b=0.164 \tag{50}$$

have also been determined using a least-squares minimization.

In Fig. 5 and Fig. 6 the ansatz (48)-(49) is compared with the values obtained by a numerical integration of eqns. (46). The prediction of eqn. (50) is shown by the solid line in Fig. 2. It can be concluded that the equations (48)-(50) give a reasonable approximation of the numerical data.

Finally, one obtains the following approximation of the isotropic Reuss bound

$$\bar{\Psi}^{RI}(\bar{\boldsymbol{\tau}}') \approx \frac{\dot{\gamma}_0 \tau^C N}{m}\left(\frac{\|\bar{\boldsymbol{\tau}}'\|}{\tau^C}\right)^m \Gamma(0,m)\exp\left(1-\cosh\left(\beta(m)\,|\,III^*\,|\right)\right), \tag{51}$$

$$\Gamma(0,m) \approx 10^{a-b(m-2)}, \tag{52}$$

$$\beta(m) \approx c\sqrt{m-2}. \tag{53}$$

Eqn. $(51)_1$ can be equivalently formulated in terms of the stress deviator $\bar{\boldsymbol{\tau}}'$

$$\boxed{\bar{\Psi}^{RI}(\bar{\boldsymbol{\tau}}') \approx \frac{\dot{\gamma}_0 \tau^C N\, \Gamma(0,m)}{m} \left(\frac{\|\bar{\boldsymbol{\tau}}'\|}{\tau^C}\right)^m \exp\left(1-\cosh\left(\beta(m)\frac{|\det(\bar{\boldsymbol{\tau}}')|}{\|\bar{\boldsymbol{\tau}}'\|^3}\right)\right)} \tag{54}$$

The approximation (54) of the isotropic Reuss bound gives a Mises type flow behavior for $m = 2$ because of $\beta(m = 2) = 0$. Such a Mises type behavior is characterized by the fact that the traceless part of the rate of deformation is proportional to the Kirchhoff stress deviator. For all values of m larger than 2 the third principal invariant of the stress deviator influences the direction of the plastic flow. This can be easily seen, if the following relations are taken into account

$$\frac{\partial\|\bar{\boldsymbol{\tau}}'\|}{\partial\bar{\boldsymbol{\tau}}'} = \frac{\bar{\boldsymbol{\tau}}'}{\|\bar{\boldsymbol{\tau}}'\|}, \qquad \frac{\partial\det(\bar{\boldsymbol{\tau}}')}{\partial\bar{\boldsymbol{\tau}}'} = (\bar{\boldsymbol{\tau}}'^2)'. \tag{55}$$

As a result, the rate of deformation has the following form

$$\boxed{\bar{\boldsymbol{D}}'^{RI} = \frac{\partial\bar{\Psi}^{RI}(\|\bar{\boldsymbol{\tau}}'\|,\det(\bar{\boldsymbol{\tau}}'))}{\partial\bar{\boldsymbol{\tau}}'} = \frac{\partial\bar{\Psi}^{RI}(\|\bar{\boldsymbol{\tau}}'\|,\det(\bar{\boldsymbol{\tau}}'))}{\partial\|\bar{\boldsymbol{\tau}}'\|}\frac{\bar{\boldsymbol{\tau}}'}{\|\bar{\boldsymbol{\tau}}'\|} + \frac{\partial\bar{\Psi}^{RI}(\|\bar{\boldsymbol{\tau}}'\|,\det(\bar{\boldsymbol{\tau}}'))}{\partial\det(\bar{\boldsymbol{\tau}}')}(\bar{\boldsymbol{\tau}}'^2)'} \tag{56}$$

where the scalar derivatives can be estimated by the approximations (48), (49), and (50).

For $m \to \infty$ the isotropic Reuss bound approaches the Tresca yield surface since the stress state is homogeneous and each orientation of a slip system occurs with the same probability. In Fig. 7 the lines of equal dissipation as predicted by eqn. (54) are shown in the Haigh-Westergaard stress space for different values of m. Also the Tresca yield criterion is plotted, which can be formulated in terms of the principal invariants of $\bar{\boldsymbol{\tau}}'$ as follows

$$-4II^3 - 27III^2 - 9k^2II^2 - 6k^4II - k^6 = 0 \tag{57}$$

(Reuss, 1933). As mentioned before, a Mises type 'yield surface' is obtained for $m = 2$. For larger values of m the yield surface is close to the one predicted by the Bishop-Hill polycrystal model (see, e.g., Gambin, 2001). This yield surface is rounded nearby the corners of the Tresca criterion and otherwise parallel to the Tresca criterion. For values of m between 100 and 150 the ansatz (48)-(50) fails to be convex. This property is due to the approximations applied.

Application of the Approximation in Elastoplasticity. After a slight modification of eqn. (54), the approximation of $\bar{\Psi}^{RI}(\bar{\boldsymbol{\tau}}')$ can be used in the context of elastoplasticity. The stress dependent part of the yield condition for elastic-plastic materials is usually required to be positive homogeneous function of degree one in the stress tensor. The following ansatz for the yield function of an isotropic polycrystal meets this requirement

$$\boxed{\bar{\Psi}(\bar{\boldsymbol{\tau}}') = \|\bar{\boldsymbol{\tau}}'\| \exp^{\frac{1}{m}}\left(1-\cosh\left(\beta(m)\frac{|\det(\bar{\boldsymbol{\tau}}')|}{\|\bar{\boldsymbol{\tau}}'\|^3}\right)\right) - \sqrt{\frac{2}{3}}\kappa(m,\beta(m))\sigma_F} \tag{58}$$

If $\kappa(m,\beta(m))$ in (58) is chosen such that σ_F represents the critical tensile stress for all m and β, one obtains

$$\kappa(m,\beta(m)) = \exp^{\frac{1}{m}}(-2\sinh(\sqrt{6}\beta(m)/36)^2). \tag{59}$$

In elastoplasticity m should be interpreted as a shape parameter that quantifies the closeness to the Mises type behavior. Experimental findings indicate that the initial yield loci of isotropic polycrystals are between the criteria by Tresca and by Mises. The ansatz (58) allows to model such a type of yield loci.

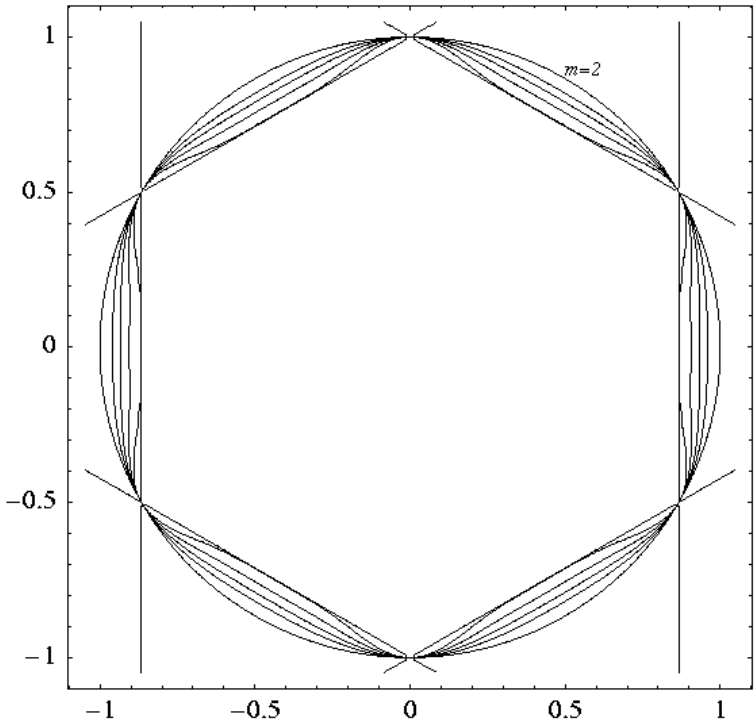

Figure 7: Approximation of $\bar{\Psi}^{RI}(\bar{\boldsymbol{\tau}}')$ for different values of m $(2, 10, 50, 100, 150)$

5 Summary and Outlook

It has been shown that the isotropic Reuss bound of the strain rate potential shows a significant dependence on the determinant of the stress deviator. This dependence implies that the viscoplastic flow is not proportional to the stress deviator. A simple analytical expression allows to reproduce the numerical findings over a wide range of strain rate sensitivities. It contains the Mises type flow behavior as a special case. Such an analytical expression for the strain rate potential can be used in order to specify the flow direction of viscoplastically isotropic polycrystals. It can also be used to specify the flow condition of elastoplastic materials. Further work should concern the isotropic Voigt bound and the influence of inhomogeneities of the crystallite orientation distribution on the flow direction. Here simple models are needed which allow for a specification of the flow direction as a function of the texture coefficients.

Acknowledgment

The authors would like to express their gratitude to Prof. A. Krawietz for his helpful comments.

References

Beran, M.: *Statistical Continuum Theories*. Interscience Publishers (1968).

Berntsen, J.; Espelid, T.: An adaptive algorithm for the approximate calculation of multiple integrals. *ACM Transactions on Mathematical Software*, 17, 4, (1991a), 437–451.

Berntsen, J.; Espelid, T.: Algorithm 698: DCUHRE: An adaptive multidimensional integration routine for a vector of integrals. *ACM Transactions on Mathemaical Software*, 17, 4, (1991b), 452–456.

Bishop, J.; Hill, R.: *Phil. Mag.*, 42, 414, (1951), 1298.

Bunge, H.-J.: Zur Darstellung allgemeiner Texturen. *Z. Metallkde.*, 56, (1965), 872–874.

Gambin, W.: *Plasticity and Textures*. Kluwer Academic Publishers (2001).

Gel'fand, I.; Minlos, R.; Shapiro, Z.: *Representations of the Rotation and Lorentz Groups and their Applications*. Oxford: Pergamon Press (1963).

Hutchinson, J.: Bounds and self-consistent estimates for creep of polycrystalline materials. *Proc. R. Soc. Lon.*, A 348, (1976), 101–127.

Kocks, U.; Mecking, H.: Physics and phenomenology of strain hardening: The FCC case. *Progr. Mat. Sci.*, 48, (2003), 171–273.

Nemat-Nasser, S.; Hori, M.: *Micromechanics: Overall Properties of Heterogeneous Materials*. Elsevier, 2 edn. (1999).

Ponte Castañeda, P.: The effective mechanical properties of nonlinear isotropic composites. *J. Mech. Phys. Solids*, 39, (1991), 45–71.

Ponte Castañeda, P.: New variational principles in plasticity and their application to composite materials. *J. Mech. Phys. Solids*, 40, 8, (1992), 1757–1788.

Ponte Castañeda, P.; Suquet, P.: Nonlinear composites. *Advances in Applied Mechanics*, 34, (1998), 171–302.

Reuss, A.: Berechnung der Fließgrenze von Mischkristallen auf Grund der Plastizitätsbedingung für Einkristalle. *Z. Angew. Math. Mech.*, 9, (1929), 49–58.

Reuss, A.: Vereinfachte Berechnung der plastischen Formänderungsgeschwindigkeiten bei Voraussetzung der Schubspannungsfließbedingung. *Z. Angew. Math. Mech.*, 13, 5, (1933), 356–360.

Roe, R.: Description of crystalline orientation of polycrystalline materials. III. General solution to pole figure inversion. *J. Appl. Phys.*, 36, (1965), 2024–2031.

Sachs, G.: Zur Ableitung einer Fließbedingung. *Z. Verein dt. Ing.*, 72, (1928), 734–736.

Taylor, G.: Plastic strain in metals. *J. Inst. Metals*, 62, (1938), 307–324.

Torquato, S.: *Random Heterogeneous Materials: Microstructures and Macroscopic Properties*. Springer (2002).

Voigt, W.: Über die Beziehung zwischen den beiden Elastizitätskonstanten isotroper Körper. *Wied. Ann.*, 38, (1889), 573–587.

Willis, J.: The structure of overall constitutive relations of nonlinear composites. *IMA Journal of Applied Mathematics*, 43, (1989), 231–242.

Zheng, Q.-S.; Fu, Y.-B.: Orientation distribution functions for microstructures of heterogeneous materials: II Crystal Distribution functions and irreducible tensors restricted by various material symmetries. *Appl. Math. Mech.*, 22, 8, (2001), 885–903.

Address: Thomas Böhlke, Albrecht Bertram, Otto-von-Guericke-Universität Magdeburg, Institut für Mechanik, PSF 4120, D-39016 Magdeburg.
email: `boehlke@mb.uni-magdeburg.de`